AADE-19-NTCE-095

Modeling the Effect of Axial Oscillation Tools in Torque and Drag Computations

Mohamed Mahjoub, Ngoc-Ha Dao and Stéphane Menand, DrillScan

Abstract

When drilling complex wells, such as those with long lateral sections, the friction forces become significantly high, which can impede advancement of the drill string and reduce drilling performance. In these situations, Axial Oscillation Tools (AOT) could be used to introduce an axial vibration to the drill string. By locally reducing the friction forces, better transmission of weight to the drill bit is possible and an increase in the rate of penetration occurs. However, to optimize the use of these tools, predictive modeling is necessary to assess their effect on drilling characteristics.

A new modeling approach is proposed to accurately model the effect of the AOT on drilling operations without the need to carry out resource-intensive and time-consuming dynamic computations. To estimate the influence length (*i.e.* the extent of the axial vibrations) and the maximum displacement at the AOT, a study was performed to determine the most important parameters. Based on this study and on the theory of wave propagation, new analytic expressions are proposed. Once the influence length and the maximum displacement are calculated, an effective friction coefficient is estimated as the mean value of the instantaneous friction coefficient and used in a stiff-string torque and drag model.

The model was applied to a real case study, and an agreement between the modeling results and field measurements regarding the influence of the AOT was obtained. Moreover, the effect of the excitation force and rate of penetration on the drill string tension profile was investigated. This work should enable drilling engineers to better optimize the position of AOT along the drill string and to maximize its efficiency.

Introduction

With the increasing complexity of well trajectories to reach deeper and farther targets, the drilling operations have become more and more challenging. For trajectories with long lateral sections, the friction forces between the drill string and wellbore are particularly high, which may significantly reduce drilling performance. Namely, the rate of penetration (ROP) and weight on bit (WOB) decrease due to drag forces, and the risk of buckling become higher due to the compression in the drill string (Menand et al. 2006, 2009).

The axial oscillation tools (AOT) are commonly used recently as a solution to try to mitigate these problems. These tools introduce an axial vibration in the drill string to locally reduce the friction coefficient, and consequently improve the transmission of weight to the drill bit. In fact, the AOT induces locally a change of the axial speed direction with time (up and down). Consequently, the friction force also changes of direction with time, which, on average, become close to zero. Several experimental studies and field measurement proved the efficiency of this technology (Alali and Barton 2011, Sola and Lund 2000). However, the theoretical modeling of the vibration-induced friction reduction has been less studied.

A simplistic modelling procedure may consist on applying a reduced friction coefficient for the entire drill string in a torque and drag model. Although this method may give acceptable results of the global mechanical response of the structure, it lacks theoretical justification. In fact, the reduced friction coefficient is obtained by fitting global drilling indicators, like the surface (or hook) load, and not related to the characteristics of the AOT itself. Also, this method disregards the effect of the vibration source position, and consequently cannot describe the effect of a local friction reduction around the AOT.

Newman et al. (2009) used a friction reduction method in torque and drag computations. Based on laboratory experiments, the authors considered a zero-friction coefficient close to the AOT within a given length, such that the removed friction forces equal the applied excitation force. This method reduces the local friction reduction and gives an overall agreement with field measurements of the hook load. However, assumptions were not justified theoretically, and no details on the development and usage of this method were provided in the paper.

To capture the propagation of the applied vibration in the drill string, some studies used a dynamic modeling in the time domain. Gee et al. (2015) and Wilson and Noynaert (2017) used

all the degrees of freedom in their model *i.e.* axial, torsional, and lateral. This approach is the most accurate, because it can take the maximum of the external forces acting on the drill string into consideration and allows to describe the intermittent contact with the wellbore. However, it requires very long computation time, which makes it difficult for everyday usage by drilling engineers.

Wicks et al. (2012, 2014) used a simplified dynamic modeling to reduce the computation time. They considered only the axial displacement and assumed that the contacts are permanent (the normal contact forces are constant). The study allowed to determine an empirical expression to estimate the influence length of the AOT, *i.e.* the extent of the axial vibrations, as a function of the excitation force, friction coefficient, and linear contact force. However, the simulations are still slow especially for long trajectories.

Shor et al. (2015) used the transfer matrix approach to solve the axial displacement problem in the frequency domain. The equation of motion was simplified by neglecting the transient phase and assuming permanent contact and harmonic displacement. Consequently, a fast resolution in the frequency domain is possible. The friction forces are modeled in that paper by a damping coefficient, calculated as a function of normal contact force, friction coefficient, excitation frequency, and an assumed displacement magnitude. Although this method can provide fast computations, to our knowledge, this model has not been coupled to a torque and drag model.

In this work, a new modeling approach is proposed to determine the impact of an AOT in torque and drag modeling. The main idea is to move from the dynamic to static framework by considering an averaged solution. More precisely, the friction coefficient used in the static torque and drag computations is obtained by averaging the instantaneous friction coefficient in the dynamic problem over one period. First, using some simplifications, an analytical resolution of the axial oscillation problem was conducted to characterize the influence length and the maximum displacement at the AOT. Then, a parametric study using 1D dynamic simulations is carried out to examine the validity of the obtained analytical expressions. By assuming a harmonic solution and that the axial displacement decreases from the maximum displacement at AOT to zero within the influence length, the displacement and speed rate can be characterized in all the structure. Finally, an expression of the friction coefficient as a function of the speed rate is used to obtain an averaged friction coefficient, which can be used in a torque and drag model.

In the first section of this paper, the modeling approach is explained, and an example of a mass-spring system is studied to illustrate the proposed averaging idea. Afterwards, the AOT influence length and maximum displacement are analytically and numerically characterized. Finally, the modeling approach is applied to a real case with field measurements, where the trajectory presents a long horizontal section, and the effect of the AOT on drag results are discussed.

Modeling approach from dynamic to static analyses

During drilling operations, the drill string is subjected to different external forces, namely the gravity, fluid pressure, and contact with the wellbore. These solicitations may be considered in a torque and drag model to determine the static position and reaction forces. However, when the drill string is subjected to an axial harmonic excitation caused by an AOT, the problem is not static anymore, and a dynamic analysis is necessary.

1D dynamic problem

A reasonable problem simplification to model the axial vibrations is to assume that the normal contact forces calculated statically without an AOT remain constant. Moreover, one can consider only the axial motion and disregard the lateral and torsional degrees of freedom in the dynamic analysis. The axial friction force F_a is expressed in terms of the normal contact force F_n as

$$F_a = \mu(V_g)\, F_n$$

$$\text{with} \quad \mu(V_g) = \operatorname{sgn}(V_g)\left[\mu_d + (\mu_s - \mu_d)\exp\left(-\frac{|V_g|}{V_g^0}\right)\right] \quad (1)$$

where μ is the friction coefficient, V_g is the slip velocity, μ_d and μ_s are the dynamic and static friction coefficient, respectively, and V_g^0 is a model parameter (see Figure 1). For simple geometries, those contact forces are almost equivalent to a distributed contact force $f_n = \rho g A \sin i$, where ρ is the density, g is the gravitational field strength, A is the cross section, and i is the inclination.

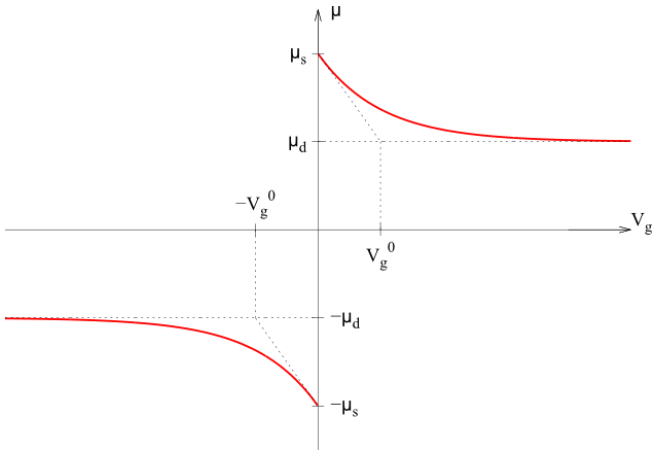

Figure 1 Representation of the friction coefficient as a function of the slip velocity.

For the static position (without AOT), the slip velocity is equal to the rate of penetration $V_g = ROP$ and the friction coefficient is $\mu(ROP)$. When the AOT is considered, then the slip velocity becomes $V_g = ROP + \dot{u}$, where u is the axial

displacement relative to the static position, and the friction coefficient is $\mu(ROP + \dot{u})$. Because the displacement u is defined relative to the static position, its equation of motion could be written with the difference between the actual forces and the forces used in the static problem. Consequently, all the constant forces disappear, and the only remaining forces are the excitation force $F_e \sin(\omega_e t)$, where F_e is the amplitude and ω_e is the angular frequency, and the relative friction forces

$$f_a = [\mu(ROP + \dot{u}) - \mu(ROP)]F_n \quad (2)$$

This problem could be solved using the finite element method, which leads to a system of equations that may be written in the following form:

$$[M]\ddot{\vec{u}} + [K]\vec{u} = \overrightarrow{f_a} + \overrightarrow{F_e} \quad (3)$$

where $\vec{u}$, $\overrightarrow{f_a}$, and $\overrightarrow{F_e}$ are, respectively, the vectors of nodal displacements, relative friction forces, and excitation forces (0 everywhere except the AOT node) and $[M]$ and $[K]$ are, respectively, the mass and stiffness matrices.

Averaged static problem

Because the excitation force and the resulting axial displacement are periodic, the proposed idea in this work is to eliminate the time dependency of the problem by considering an averaged static problem. At each position x with respect to the AOT, the axial displacement may be written as

$$u(x,t) = U(x)\sin\big(\omega_e t - \varphi(x)\big) \quad (4)$$

where $U(x)$ and $\varphi(x)$ are, respectively, the displacement amplitude and phase shift at the position x. From this equation, the speed rate could be deduced as $\dot{u} = \omega_e u_1$ with $u_1(x,t) = U(x)\sin(\omega_e t - \varphi(x) - \pi/2)$. Hence, the instantaneous friction coefficient becomes $\mu(x,t) = \mu\big(ROP + \omega_e u_1(x,t)\big)$ and the averaged friction coefficient could be given by

$$\bar{\mu}(x) = \frac{\omega_e}{2\pi}\int_0^{2\pi/\omega_e} \mu(x,t)\ \mathrm{d}t$$
$$= \frac{\omega_e}{2\pi}\int_0^{2\pi/\omega_e} \mu(ROP + \omega_e U(x)\sin(\omega_e t))\,\mathrm{d}t \quad (5)$$

where the shift $\varphi(x)$ disappears because the sin function is periodic. Once $\bar{\mu}(x)$ is obtained, one can carry out a normal torque and drag computation to examine the effect of the AOT-induced friction reduction. The only remaining unknown in this equation is the function $U(x)$. To define it, we assume that the displacement amplitude decreases linearly from a maximum displacement u_{max} at the AOT to 0 within an influence length L such that

$$U(x) = \begin{cases} u_{max}\left(1 - \dfrac{2\,|x|}{L}\right) & \text{if} \quad -L/2 \le x \le L/2 \\ 0 \quad \text{elsewhere} \end{cases} \quad (6)$$

This means that one has only to characterize the influence length and the maximum displacement to define the averaged friction coefficients in all the structure.

Mass-spring-friction system

To better understand the averaging idea, we consider a system with a mass m and a spring with stiffness k (see Figure 2) moving with a global speed ROP. The natural frequency is $\omega_0 = \sqrt{k/m}$. The system is subjected to the excitation force $f_e = F_e \sin(\omega_e t)$ and the relative friction between the mass and the floor $f_a = [\mu(ROP + \dot{u}) - \mu(ROP)]F_n$. If we assume that there is no difference between the static and dynamic friction coefficients ($\mu_s = \mu_d$), then the friction force reduces to $f_a = 0$ when $ROP + \dot{u} > 0$ and to $f_a = -2\mu_s F_n$ when $ROP + \dot{u} < 0$. Therefore, one can find an analytical solution for this problem depending on the sign of $ROP + \dot{u}$.

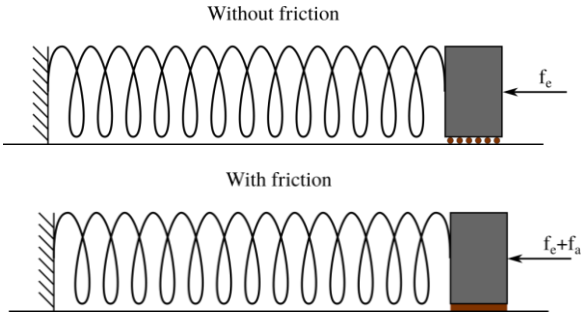

Figure 2 Schematic representation of the spring-mass system with or without friction.

We consider the following numerical values:

- $k = (2\pi)^2$ N/m and $m = 1$ kg $\Rightarrow$ $\omega_0 = \sqrt{k/m} = 2\pi$ rd/s $\Rightarrow T_0 = 2\pi/\omega_0 = 1$ s;
- $\mu_s = \mu_d = 0.3$, $ROP = 0.001$ m/s, $F_e = 10$ N, and $F_n = -20$ N;
- $\omega_e = 2\omega_0$, $4\omega_0$, or $8\omega_0$.

Figure 3(a) shows the obtained results for the displacement for different excitation frequencies. As can be seen, after a transient regime, the system reaches a stabilized status, where the displacement is oscillating around an average value. Moreover, because the average friction force is positive (see Figure 3(b)) and the average excitation force is 0, the average displacement is positive. This means that, under the effect of the excitation force, the friction-induced-compression in the spring was reduced from its initial value caused by the global speed ROP. It is that same average friction reduction phenomena that we are looking for in the case of drill strings.

Analytical and numerical characterization of the AOT influence length and maximum displacement

To find analytical expressions relating the AOT influence length and maximum displacement to the other problem parameters, both theoretical developments and numerical simulations were employed. Using some problem simplifications, the theoretical developments provide candidate formulae, which are compared to the numerical simulation results to examine their validity.

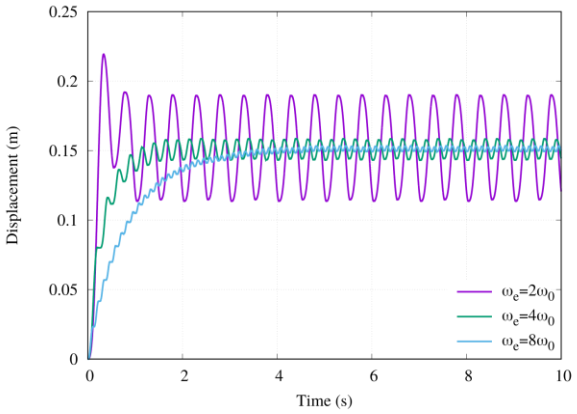

(a) Displacement.

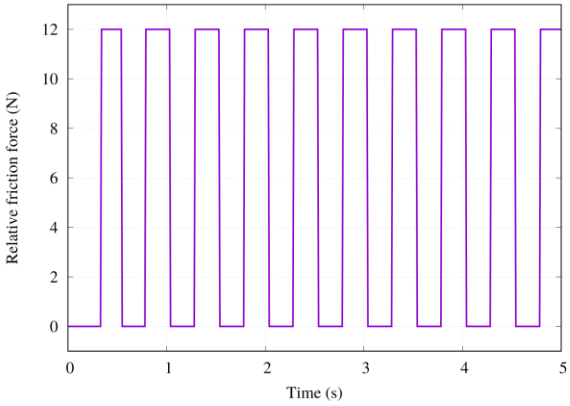

(b) Relative friction force for $\omega_e = 2\omega_0$.

Figure 3 Response of the spring-mass-friction system for different excitation frequencies.

Wave propagation solution

When the contact forces f_a are assumed to be distributed over the whole structure, the equation of motion describing the axial displacement of drill string becomes:

$$EA\frac{\partial^2 u}{\partial x^2} + f_a = \rho A\frac{\partial^2 u}{\partial t^2} \tag{7}$$

where E is the Young modulus, A is the cross-section area, and ρ is the density. This equation is similar to d'Alembert wave equation, in which $c = \sqrt{E/\rho}$ is the wave propagation speed. The only difference is the presence of the friction force f_a which will attenuate the wave amplitude. Because this force is highly non-linear, it is difficult to analytically solve this wave equation. Here, we make some simplifications on f_a to enable the analytic computations. We assume that the solution of Eq. (7) could be written in the following form:

$$u(x,t) = u_{max}\left(1 - \frac{2|x|}{L}\right)\sin\left(\omega_e\left(t - \frac{|x|}{c}\right) - \phi\right)$$
$$\text{if} \quad -L/2 \le x \le L/2 \quad \text{and} \quad 0 \quad \text{elsewhere} \tag{8}$$

where u_{max} is the maximum displacement at $x = 0$, L is the influence length, and ϕ is the phase shift between the excitation force ($F_e \sin(\omega_e t)$) and the displacement. Figure 4 shows an example of the shape of the displacement $u(x,t)$.

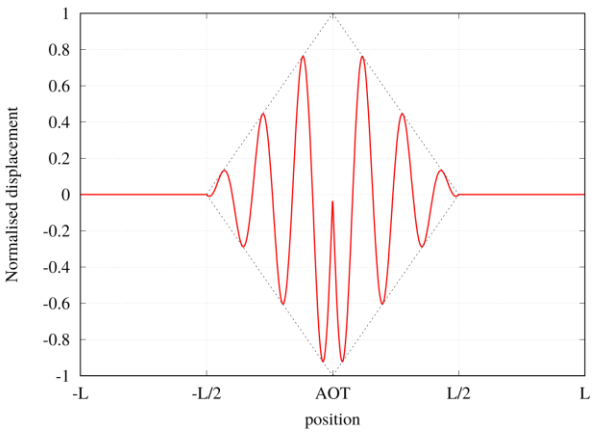

Figure 4 Example of the shape of the displacement function.

By neglecting the difference between static (μ_s) and dynamic (μ_d) friction coefficients ($\mu = \mu_s = \mu_d$ in Eq. **1**) and after some developments, the following expressions are found:

$$L = 2\sqrt{\lambda_F^2 - \lambda^2} \qquad \text{and} \qquad u_{max} = \frac{F_e}{EA}\frac{\lambda}{2\lambda_F}\sqrt{\lambda_F^2 - \lambda^2} \tag{9}$$

where we identified the wave characteristic length $\lambda = c/\omega_e = \sqrt{E/\rho}/\omega_e$ and the force characteristic length $\lambda_F = \frac{F_e}{\mu f_n}$. We can see that when $\lambda \ll \lambda_F$, we find the expression $L = \frac{2F_e}{\mu f_n}$, which is used in the literature (Wicks, et al., 2012; 2014). However, when $\lambda > \lambda_F$, the expressions (9) are not valid anymore and another solution is needed.

Quasi-static solution

For big values of λ, the effect of inertia is reduced, and the quasi-static assumption might be made. Hence, we can write the equilibrium of the external forces by neglecting the inertia effects (the acceleration) as $F_e = \mu f_n L$, which leads to

$$L = \lambda_F \qquad \text{and} \qquad u_{max} = \frac{F_e}{EA}\frac{\lambda_F}{8} \tag{10}$$

Piece-wise solution

To get an analytical solution that provides a good description of the problem for all the ranges of λ_F and λ, Eqs. (9) and (10) are combined into the following expressions:

$$L = \begin{cases} \lambda_F & \text{if} \quad \lambda_F \leq \alpha\lambda \\ 2\sqrt{\lambda_F^2 - \lambda^2} & \text{if} \quad \lambda_F \geq \beta\lambda \\ \lambda + a(\lambda_F - \lambda) & \text{if} \quad \alpha\lambda < \lambda_F < \beta\lambda \end{cases} \quad \text{and}$$

$$u_{max} = \frac{F_e}{EA} \begin{cases} \lambda_F/8 & \text{if} \quad \lambda_F \leq \alpha\lambda \\ \frac{\lambda}{2\lambda_F}\sqrt{\lambda_F^2 - \lambda^2} & \text{if} \quad \lambda_F \geq \beta\lambda \\ \lambda/8 + b(\lambda_F - \lambda) & \text{if} \quad \alpha\lambda < \lambda_F < \beta\lambda \end{cases} \quad (11)$$

where α, β, a, and b are numerical constants, which will be determined based on the numerical simulation results.

Validation on numerical simulations

A series of dynamic computations using a finite element code were performed to examine the validity of the analytical expressions developed above. Different problem parameters were varied during this parametric study, namely the excitation force amplitude and frequency, friction coefficients, inclination (and consequently contact forces), rigidity, and drill string length (see Table 1 for the list of parameter combinations). Since the number of simulations is high, we chose short drill strings without tool-joints (200 m and 500 m) and a simple geometry (straight line with well diameter $WD = 16$ cm and drill string inner and outer diameters $ID = 8$ cm and $OD = 12$ cm) to ensure reasonable computation time. However, for the application section, a real scale drill string is employed.

For each parameter combination, the normal contact forces are computed using a stiff-string torque and drag model and used in the dynamic computations of the axial motion of the drill string like described in the first section (with $ROP = 0$). After each simulation, an envelope of the axial displacement is obtained from the node displacements at different time steps (see for example Figure 5). Then, the influence length and the maximum displacement are automatically determined. To avoid problems related to boundary effects, all the cases where the influence length is equal to the structure length are discarded in our interpretations *i.e.* we keep only the simulations where the influence length is strictly smaller than the drill string length. By gathering these results in charts like in Figures 6 to 8, where each point represents the result of one simulation, we can have a visual comparison between the numerical dynamic results and the analytical expressions developed above.

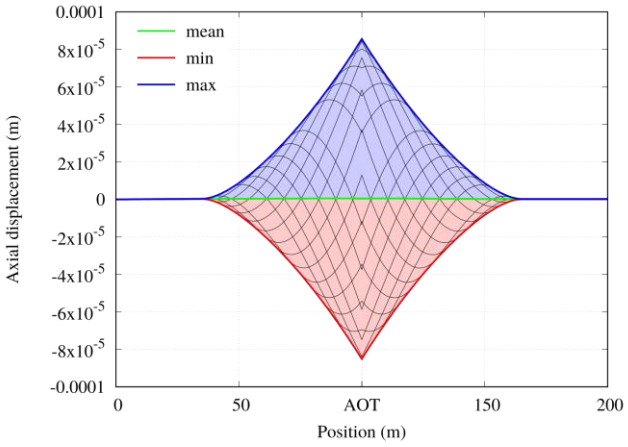

Figure 5 Example of the dynamic computation results: the black lines represent the deformed string at different time steps; and the other lines represent the envelope of the displacements.

Figure 6 shows a comparison of the influence length and maximum displacement from Eq. (11) with the numerical results. The x-axis gives the value estimated by the analytical expression; and the y-axis gives the value calculated numerically. One can affirm that the analytical expression describes well the problem if the points are close to the line y=x. As can be seen, these piece-wise defined expressions are in a good agreement with the numerical results for all the tested parameter combinations. The results given by Eq. (9) are in a good agreement with the numerical results for high values of λ_F ($\lambda_F \geq \beta\lambda$), whereas the results given by Eq. (10) are in a good agreement with the numerical results for low values of λ_F ($\lambda_F \leq \alpha\lambda$).

Table 1 List of parameter combinations used in the parametric study.

<table>
<tr><th>Length</th><th>Dynamic friction</th><th>Young modulus</th><th>Angular frequency</th><th>Other parameters</th></tr>
<tr><td rowspan="5">200 m</td><td rowspan="4">$\mu_d = 0.2 \leq \mu_s$</td><td rowspan="3">$E = 210$ GPa</td><td>$\omega_e = 100$ rd/s</td><td rowspan="5">All combinations with
F_e from 1 to 10 kN every 1kN
μ_s from 0.2 to 0.4 every 0.05
i from 10 to 90° every 10°</td></tr>
<tr><td>$\omega_e \times 2$</td></tr>
<tr><td>$\omega_e \times 4$</td></tr>
<tr><td>$E \times 2$</td><td rowspan="3">ω_e</td></tr>
<tr><td>$E / 2$</td></tr>
<tr><td>$\mu_d = \mu_s$</td><td rowspan="2">E</td></tr>
<tr><td>500 m</td><td>$\mu_d = 0.2 \leq \mu_s$</td></tr>
</table>

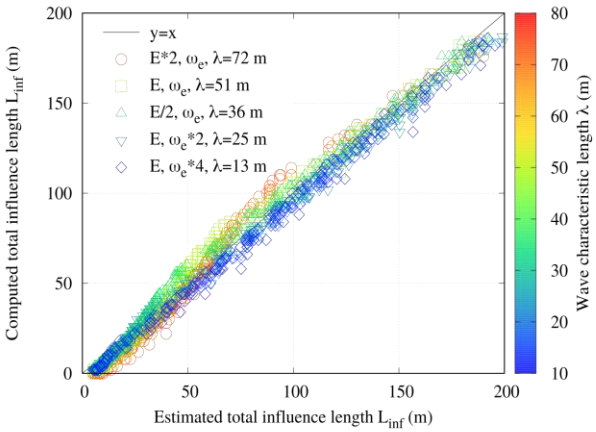

(a) Influence length.

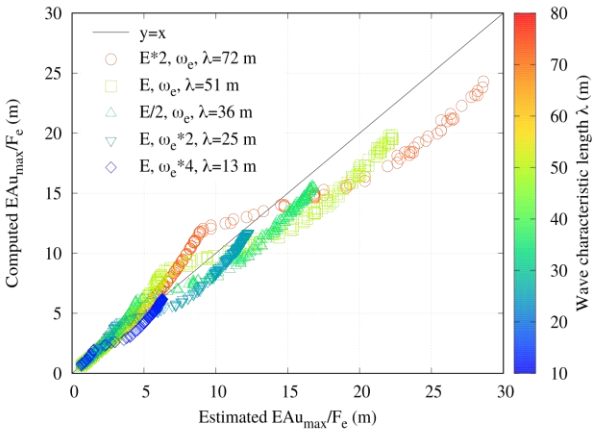

(b) Maximum displacement.

Figure 6 Comparison of the piece-wise defined formulae (11) with the numerical simulation results.

Analysis of the effect of some problem parameters

Structure length: Figure 7(a) and Figure 8(a) show a comparison of the numerical results for two drill string lengths (200 m and 500 m) along with the theoretical predictions from Eq. (11). It is clear that, as long as the AOT vibrations are far from the boundaries (the influence length in Figure 7(a) is below 200 m), the structure length has no effect on the results. This means that the vibration effect depends on the contact forces and drill string materials close to the AOT only. One can also notice from this figure that the theoretical predictions of the maximum displacement become closer to the numerical results for the higher values of λ_F. This remark is encouraging knowing that in most of the practical cases, we have $\lambda_F \gg \lambda$.

Dynamic friction coefficient: The effect of the dynamic friction coefficient is investigated in Figure 7**(**b) and Figure

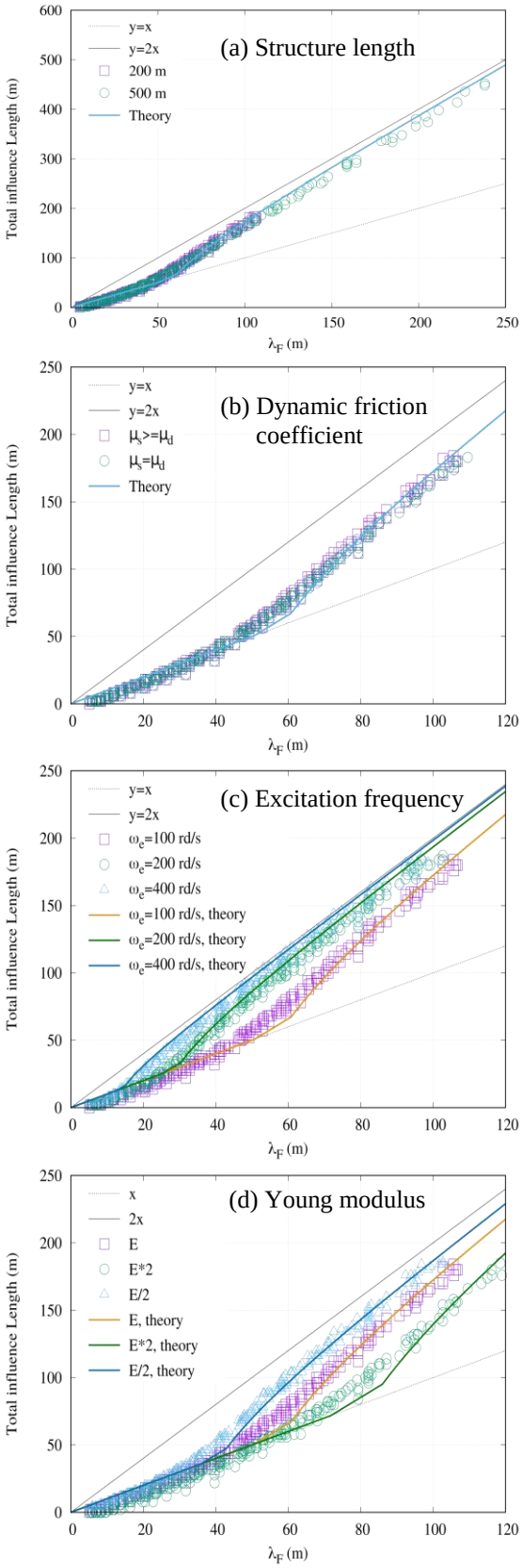

Figure 7 Effect of some problem parameters on the influence length.

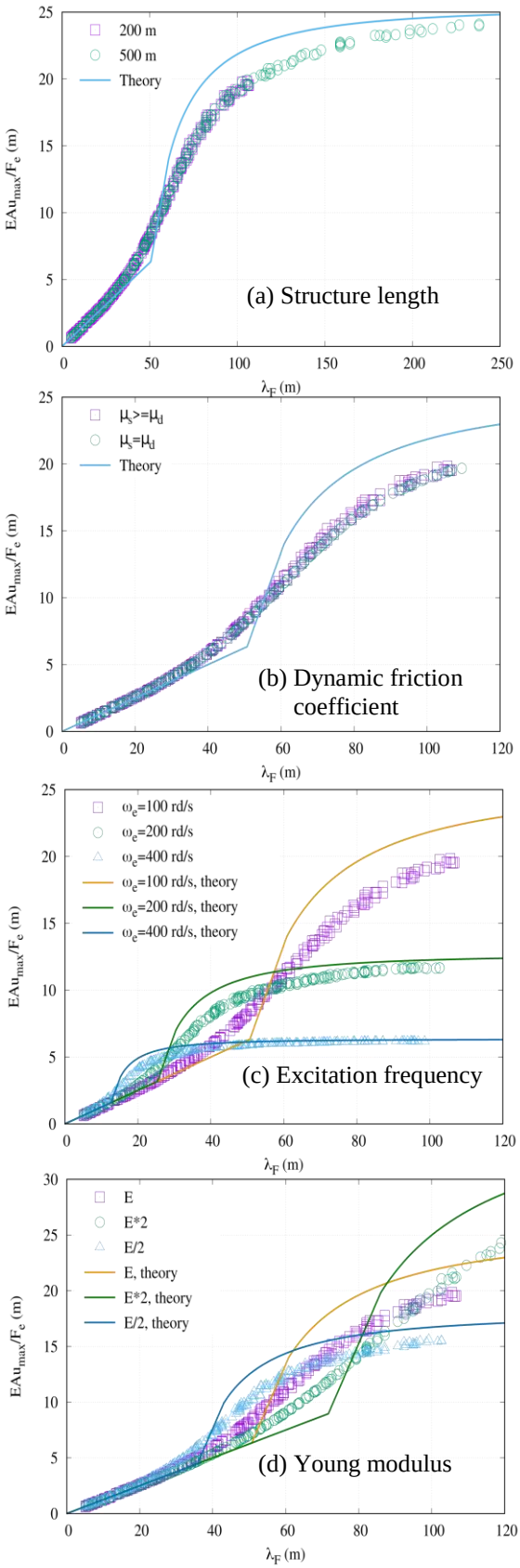

Figure 8 Effect of some problem parameters on the maximum displacement.

8(b), where two series of simulations are compared: the first with different values for the dynamic and static friction coefficients (constant dynamic coefficient $\mu_d = 0.2 \leq \mu_s$) and the second with the same values for the dynamic and static friction coefficients ($\mu_d = \mu_s$). The distinction between the static and dynamic coefficients has no significant influence on the results. This means that the AOT friction reduction is due mainly to the change of speed direction (up and down) rather than the speed amplitude.

Excitation frequency and Young modulus: Figure 7 (c and d) and Figure 8(c and d) represent the effect of the excitation frequency and the string rigidity. These two parameters have complementary effects as they are linked in the definition of the wave characteristic length ($\lambda = \sqrt{E/\rho}/\omega_e$). One can notice that the Influence length is enhanced for higher excitation frequencies or smaller Young moduli *i.e.* smaller values of λ. This remark is very important for the design of an AOT. In fact, contrarily to the available influence length expression in the literature ($L = 2\lambda_F$), where only the excitation force amplitude is considered, the developed expression in this paper provides a supplementary information about the impact of the force frequency.

Case Study

The new developed AOT model is applied to a case study with a typical unconventional well. As shown in Figures 9 and 10, the well trajectory is composed of a quasi-vertical section followed by a long lateral section. In this study, we focus only on the lateral section, where two bottomhole assemblies (BHAs) were used (see Tables **2** and **3**). The first BHA (#1) was not equipped with an AOT, whereas the other BHA (#2) was equipped with a 20 klbf amplitude and 15 Hz frequency AOT. Like the previous section, a series of stiff-string torque and drag computations are conducted to examine the impact of the AOT presence in the BHA. For the numerical simulations, the friction coefficient is calibrated to 0.1 for the cased part (above MD 3237m) and 0.2 for the open hole. Unfortunately, no downhole vibration data along the BHA was available to have a more accurate comparison with the model.

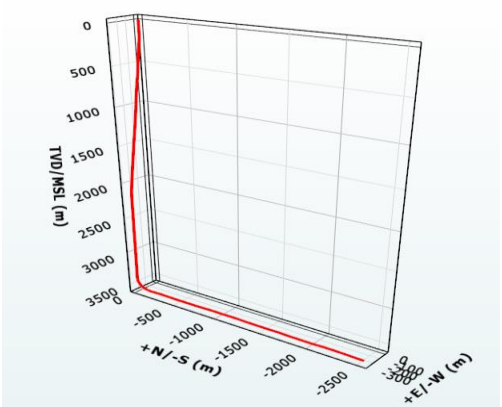

Figure 9 3D view of the well trajectory for the case study

Table 2 BHA #1 not equipped with an AOT.

Type	Length	OD	ID	Tooljoint OD	Gauge	Total length	Contact	Mass	Total mass	Linear mass
	(m)	*(inch)*	*(inch)*	*(inch)*	*(inch)*	*(m)*	*(m)*	*(kg)*	*(kg)*	*(kg/m)*
PDC	0.15	-	-	-	6 3/4	0.15	-	14.16	14.16	92.92
Steerable mud motor	8.38	4 3/4	3 3/4	-	-	8.53	-	283.40	297.56	33.81
BNT	-	-	-	-	-	-	1.45	-	-	-
Float sub x 1	1.10	4 3/4	2 3/4	-	-	9.63	-	65.47	363.03	59.66
Shoe x 1	0.82	4 3/4	2 3/8	-	-	10.45	-	55.39	418.42	67.31
MWD	9.27	4 3/4	2 3/4	-	-	19.72	-	552.85	971.27	59.66
Sensor package	-	-	-	-	-	-	11.98	-	-	-
DC x 1	9.24	4 1/2	2 3/4	-	-	28.96	-	466.08	1437.35	50.47
XO x 1	0.91	5 1/4	2 3/4	-	-	29.87	-	72.74	1510.09	79.55
DP to surface	9.66	4	3	5	-	39.53	-	292.31	1802.40	30.26

Table 3 BHA #2 equipped with an AOT.

Type	Length	OD	ID	Tooljoint OD	Gauge	Total length	Contact	Mass	Total mass	Linear mass
	(m)	*(inch)*	*(inch)*	*(inch)*	*(inch)*	*(m)*	*(m)*	*(kg)*	*(kg)*	*(kg/m)*
PDC	0.15	-	-	-	6 3/4	0.15	-	14.16	14.16	92.92
Steerable mud motor	8.23	5	3 3/4	-	-	8.38	-	358.03	372.19	43.51
BNT	-	-	-	-	-	-	1.41	-	-	-
Float sub x 1	1.10	4 3/4	2 3/4	-	-	9.48	-	65.47	437.66	59.66
Shoe x 1	0.82	4 3/4	2 3/8	-	-	10.30	-	55.39	493.06	67.31
MWD	9.27	4 3/4	2 3/4	-	-	19.57	-	552.85	1045.91	59.66
Sensor package	-	-	-	-	-	-	11.83	-	-	-
DC x 1	9.24	4 3/4	2 3/4	-	-	28.80	-	551.03	1596.94	59.66
XO x 1	0.91	5 1/4	2 3/4	-	-	29.72	-	72.74	1669.68	79.55
DP x 62	598.86	4	3	5	-	628.58	-	18123.03	19792.71	30.26
AOT x 1	3.41	4 7/8	2	-	-	632.00	-	268.39	20061.10	78.62
Sub x 1	3.14	4 7/8	2	-	-	635.14	-	246.83	20307.93	78.62
DP to surface	9.66	4	3	5	-	644.80	-	292.31	20600.24	30.26

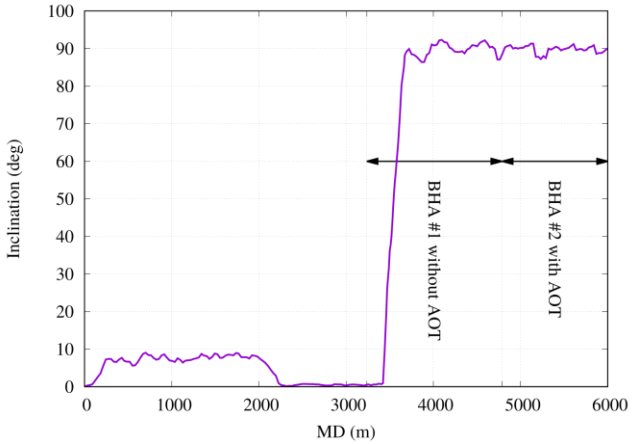

Figure 10 Measured depth (MD) vs. Inclination.

Figure 11 shows a comparison between the field data and simulation results for the surface load. The data represents only the sliding, where the AOT is used. The drill string is moving with an ROP of approximately 20 ft/h with a WOB of approximately 15 klbf. The difference between the curves "Sim. no AOT" and "Sim. AOT" is whether the AOT in the second BHA (below 4788 m) is activated or not. As expected, the presence of the AOT in the BHA induces a clear increase of the surface tension, which is well reproduced by the model.

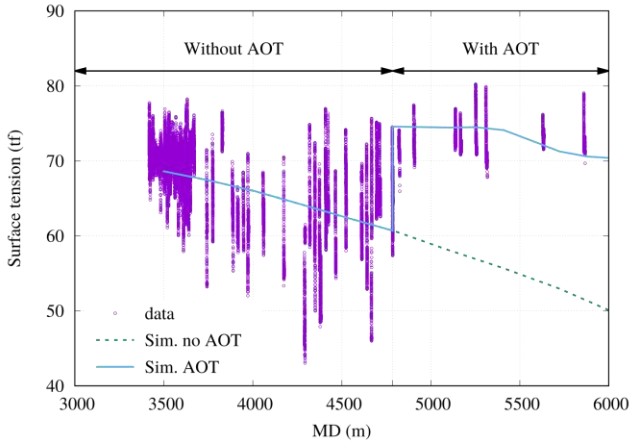

Figure 11 Variation of the surface tension with the bit depth for the horizontal section (slide drilling only).

The observed scatter in the field data can be explained by the difficulty of sliding due to friction, which can also be seen in Figure 12(a) for the WOB. It is possible to capture this by varying the friction coefficient like in Figure 12(b). It is clear that the scatter is reduced in the presence of the AOT, because the friction forces are reduced.

To better visualize the influence of the AOT, the tension profile in the drill string is presented in Figure 13 for different excitation forces and two ROP values. As the force amplitude increases, the friction in the horizontal section is reduced and

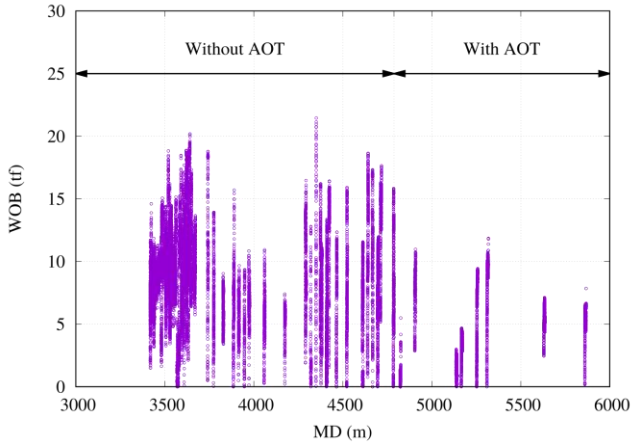

(a) Variation of WOB.

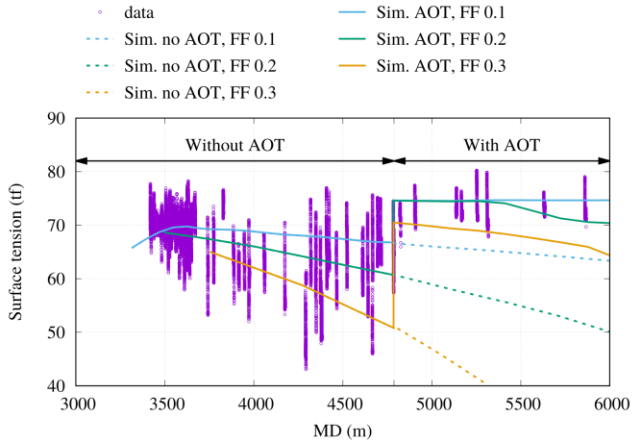

(b) Variation of the result with friction factor (FF).

Figure 12 Explanation of the surface tension scatter.

consequently, the hook-load (tension at surface) increases. Also, the intensity and the length of the compressed parts of the structure are reduced significantly, which should limit the buckling phenomena.

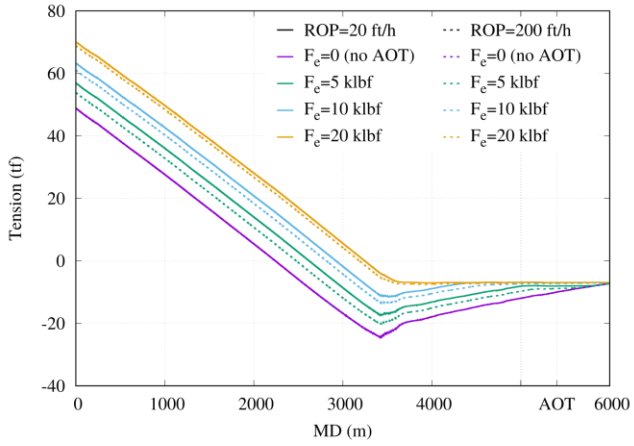

Figure 13 Tension in the drill string for different excitation force amplitudes and two ROP values.

When comparing the solid and dashed lines in Figures 13, one can notice that the impact of the AOT is reduced with the higher ROP. This result could be explained by the definition of the average friction coefficient (Eq. 5), which depends on the sign of $ROP + \dot{u}$. On the one hand, when ROP is small compared to the variation of $\dot{u}$, the positive and negative contributions of $ROP + \dot{u}$ are almost equal and the average friction coefficient is close to 0 (equal 0 when $ROP = 0$). On the other hand, for higher values of ROP, the positive contribution of $ROP + \dot{u}$ becomes more important than the negative contribution, and the friction reduction is limited. In the extreme case when $ROP > \max(\dot{u})$, the negative contribution vanishes, and the averaged friction coefficient becomes $|\bar{\mu}| \in [\mu_d, \mu_s]$, which means that the friction reduction is almost insignificant. This confirms the claim that the AOT friction reduction is due mainly to the change of speed direction (up and down) rather than the speed amplitude.

Conclusions

- A new approach is proposed to model the impact of axial oscillation tools on drill string mechanics. The modeling idea consists on transforming the dynamic solution into a static solution using an averaging procedure.
- Analytical expressions of the AOT influence length and maximum displacement are determined for both high and low frequency regimes. These expressions are validated with a series of numerical dynamic simulations, varying the parameters with the greatest influence.
- The obtained influence length and maximum displacement are used to compute averaged friction coefficient around the AOT, which can be used in stiff-string torque and drag computations.
- The model was applied to a real scale trajectory with field measurements. The studied well was drilled as a quasi-vertical section followed by an extended lateral section, where two types of BHAs were employed, with or without an AOT. The influence of the axial vibrations is clear on the surface tension, which is well reproduced by the model.
- The influence of the rate of penetration and AOT excitation force on the drill string tension was examined. It is found that the impact of the AOT increases with the excitation force amplitude and decreases with higher values of the ROP.
- Compared to complete dynamic computations, the model response may be considered as accurate enough to optimize the characteristics of the AOT and its position in the drill string, knowing the complexity and uncertainty of the modeled problem and the considerable gain of time achieved by the proposed approach. Extension of this work could be applied to other types of excitation tools that combines axial and lateral vibrations.

References

1. Alali, A. and Barton, S. P.: “Unique Axial Oscillation Tool Enhances Performance of Directional Tools in Extended Reach Applications.” Brasil Offshore Conference and Exhibition. Macaé, Brazil: Society of Petroleum Engineers, 2011.
2. Gee, R., Hanley, C., Hussain, R., Canuel, L. and Martinez, J.: “Axial Oscillation Tools vs. Lateral Vibration Tools for Friction Reduction - What's the Best Way to Shake the Pipe?” SPE/IADC Drilling Conference and Exhibition. London, United Kingdom: Society of Petroleum Engineers, 2015.
3. Menand, S., Isambourg, P., Sellami, H., Simon, C. and Bouguecha, A.: “Axial Force Transfer of Buckled Drill Pipe in Deviated Wells.” SPE/IADC Drilling Conference and Exhibition. Amsterdam, The Netherlands: Society of Petroleum Engineers, 2009.
4. Menand, S., Sellami, H., Tijani, M. and Akowanou, J.: “Buckling of Tubulars in Actual Field Conditions.” SPE Annual Technical Conference and Exhibition. San Antonio, Texas, U.S.A.: Society of Petroleum Engineers, 2006.
5. Newman, K. R., Burnett, T. G., Pursell, J. C. and Gouasmia, O.: “Modeling the Affect of a Downhole Vibrator. SPE/ICoTA Coiled Tubing and Well Intervention Conference and Exhibition. The Woodlands, Texas, USA: Society of Petroleum Engineers, 2009.
6. Shor, R. J., Dykstra, M. W., Hoffmann, O. J. and Coming, M.: “For better or worse: applications of the transfer matrix approach for analyzing axial and torsional vibration.” SPE/IADC Drilling Conference and Exhibition. London, United Kingdom: Society of Petroleum Engineers, 2015.
7. Sola, K.-I. and Lund, B.: “New Downhole Tool for Coiled Tubing Extended Reach. SPE/ICoTA Coiled Tubing Roundtable. Houston, Texas, USA: Society of Petroleum Engineers, 2000.
8. Wicks, N., Pabon, J. A. and Zheng, A. S.: “Modeling and field trials of the effective tractoring force of axial vibration tools.” SPE Deepwater Drilling and Completions Conference. Galveston, Texas, USA: Society of Petroleum Engineers, 2014.
9. Wicks, N., Pabon, J. A., Auzerais, F. M., Kats, R., Godfrey, M., Chang, Y. and Zheng, A. S.: “Modeling of axial vibrations to allow intervention in extended reach wells.” SPE Deepwater Drilling and Completions Conference. Galveston, Texas, USA: Society of Petroleum Engineers, 2012.
10. Wilson, J. K. and Noynaert, S. F.: “Inducing Axial Vibrations in Unconventional Wells: New Insights through Comprehensive Modeling.” SPE/IADC Drilling Conference and Exhibition. The Hague, The Netherlands: Society of Petroleum Engineers, 2017.